# Supporting Information for "Automated global classification of surface layer stratification using high-resolution sea surface roughness measurements by satellite synthetic aperture radar"

Justin E. Stopa[1], Chen Wang[2], Doug Vandemark[3], Ralph Foster[4], Alexis

Mouche[5], Bertrand Chapron[5]

[1]Department of Ocean Resources and Engineering, School of Ocean and Earth Science and Technology, University of Hawaiʻi at

Mānoa, USA

[2]School of Marine Sciences, Nanjing University of Information Science and Technology, Nanjing, China

[3]Ocean Processes Analysis Laboratory, University of New Hampshire, Durham, NH, USA

[4]Applied Physics Laboratory, University of Washington, Seattle, WA, USA

[5]Univ. Brest, CNRS, IRD, Ifremer, Laboratoire d'Océanographie Physique et Spatiale (LOPS), IUEM, 29280, Brest, France

**Contents of this file**

1. Text S1 to S3

2. Figures S1 to S11

**Introduction**

Section 1 (S1) describes the core datasets used in the manuscript and our method to

estimate further restrict the output of Wang, Tandeo, et al. (2019). We provide additional

June 7, 2022, 5:18am

details of the how synthetic aperture radar data is processed. In section 2 (S2), we provide an alternative set of Figures using more lenient constraints of the model threshold of 50% rather than 95% like that used in the main manuscript. In section 3 (S3), we provide additional variations of Figure 3 of the main text that have different $Ri$ constraints when mapping ERA5, show different seasons, and show the ERA5 and SAR comparison for the Northwest Indian Ocean.

**Text S1. - Extended Methods Description** In this manuscript, we rely on the image classification model of Wang, Tandeo, et al. (2019) which estimates the probability of the ten most prevalent geophysical phenomena in the WV data. The ten geophysical phenomena include:

- NV - no image variance (previously called "pure ocean waves")

- WS - Wind Streaks

- MC - Micro-scale Convection

- RC - Rain Cells

- BS - Biological Slicks

- SI - Sea Ice

- IB - Icebergs

- LW - Low Wind area

- AF - Atmospheric Front or air-mass boundary

- OF - Oceanic Front or ocean water boundary

are described in Wang, Mouche, et al. (2019). We focus on images with shallow convective cells (MC), wind-streaks (WS), and images with little or no image variance at MABL length scales (NV). We make practical use of the WV data by using a convolutional neural network (CmWV) that calculates a probability of occurrence for each of the ten most common phenomena (Wang, Tandeo, et al., 2019). The combined probabilities from all ten classes sum to unity. The phenomenon with the highest probability determines the (dominant) class of each image. To ensure the robustness of the results presented in the main manuscript, we require at least 95% probability on the MC, WS, and NV classifi-

cations. When we use we use a lower the probability of 50%, the results are not affected and the Figures and corresponding conclusions are the same as the results presented in the main manuscript. In the following section (S2), we present an identical set of Figures corresponding the main text but using a probability threshold of 50%.

CmWV has a low false alarm rate for MC and WV even when lower selection thresholds of 95% are selected. We find that CmWV sometimes misclassified other classes into the NV category. To mitigate potential misclassifications, we use spectral analysis to distinguish when the images have negligible atmospheric imprints within the MABL length scales (typically 0.8 to 4 km). Spectral analysis using a Fast Fourier Transform (FFT) shows a clear distinction between NV and WS/MC classes. In Figure SS1, we show the probability density function (PDF) of the cross-wind MABL-scale (0.8 to 4 km) spectral variance for each of these classes. Both the WS and MC classes have a broad range of variance extending from 300 $m^2$ to more than 2000 m$^2$ while the NV class contains more than 90% of its variance in the range from 20 to 500 m$^2$. To reduce the number of NV misclassifications we omit images classified as NV that had MABL variance larger than 250 m$^2$. In Figure SS2, we show the results when using the FFT information. The biggest impact is to the NV class and we reduce the dataset by a factor of two. For the WS and MC events the FFT constraint only has a minimal effect.

CmWV often misclassifies images into the ocean front or ice berg classes. This is most likely because these are rare localized features embedded in one of the more common classes (Wang, Tandeo, et al., 2019). Detecting MABL CS requires surface wind waves,

so we cannot use sea ice images. Hence, we remove these three classes and proportionally redistribute their probabilities to the remaining seven classes.

Next, we ensure that the SAR backscatter is consistent across the WV images, we require ERA5 $U_{10}^N \geq 3\ ms^{-1}$, which is just above the threshold for wind-wave generation. Wang et al. (2020) demonstrated that WS induce much stronger image contrast at the larger incidence angle. We have found that this is also true for MC and NV. Accordingly, we limit our analysis to the WV2 images.

## Text S2. - Alternative set of images using a probability of 50%

Here we provide an identical set of Figures SS3, SS4, SS5, SS6 that appear in the main manuscript but with the exception that the model probability of Wang, Tandeo, et al. (2019) is to a threshold of 50%. The results are very similar to those in the main text. Notice the increase the shading in Fig. SS4 and the increased overlap between the MC, WS, and NV classes. The regional patterns in Figs. S5, SS6 are similar to those in Figs. 3 and 4 in the main text.

## Text S3. - Variations of Figures 3 and 4 from the main text

In this section we provide different variations of the criteria used in the main text to demonstrate the minor impact on the results. Figs. S7, S8, and S9 show similar results as those in Fig. 3 of the main text but change the $Ri$ classification ranges of the ERA5 mapping.

## References

Wang, C., Mouche, A., Tandeo, P., Stopa, J. E., Longépé, N., Erhard, G., ... Chapron, B. (2019, jul). A labelled ocean sar imagery dataset of ten geophysical phenomena

from sentinel-1 wave mode. *Geoscience Data Journal*, *6*(2), 105–115. doi: 10.1002/ gdj3.73

Wang, C., Tandeo, P., Mouche, A., Stopa, J. E., Gressani, V., Longepe, N., ... Chapron, B. (2019, dec). Classification of the global sentinel-1 SAR vignettes for ocean surface process studies. *Remote Sensing of Environment*, *234*, 111457. doi: 10.1016/j.rse .2019.111457

Wang, C., Vandemark, D., Mouche, A., Chapron, B., Li, H., & Foster, R. C. (2020, dec). An assessment of marine atmospheric boundary layer roll detection using sentinel-1 SAR data. *Remote Sensing of Environment*, *250*, 112031. doi: 10.1016/j.rse.2020 .112031
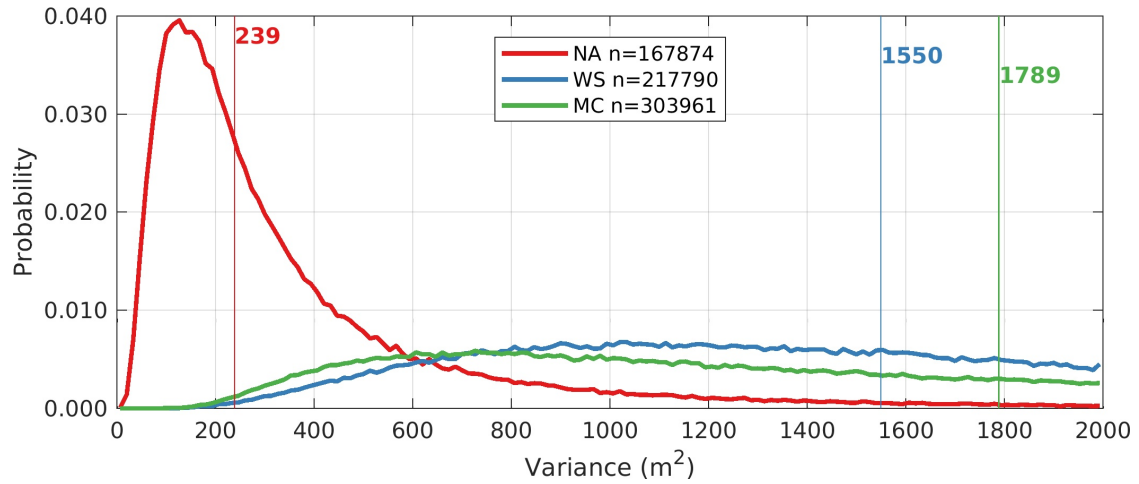
**Figure S1.** (a) PDFs of the FFT variance from 0.8 to 4 km scales for cells (unstable in green), streaks (near stable in blue), and negligible atmospheric variability (stable in red) detection from SAR. The vertical lines represent the median values.
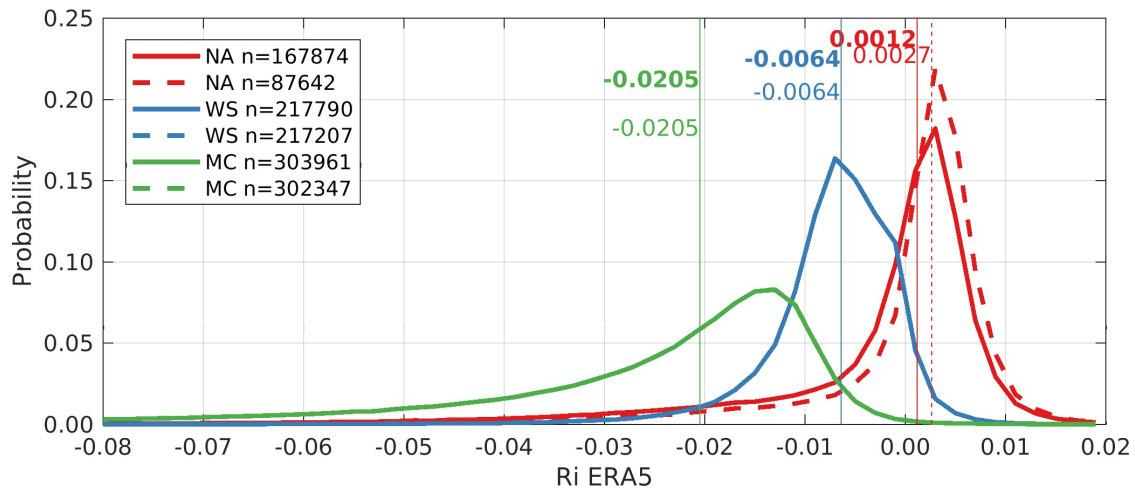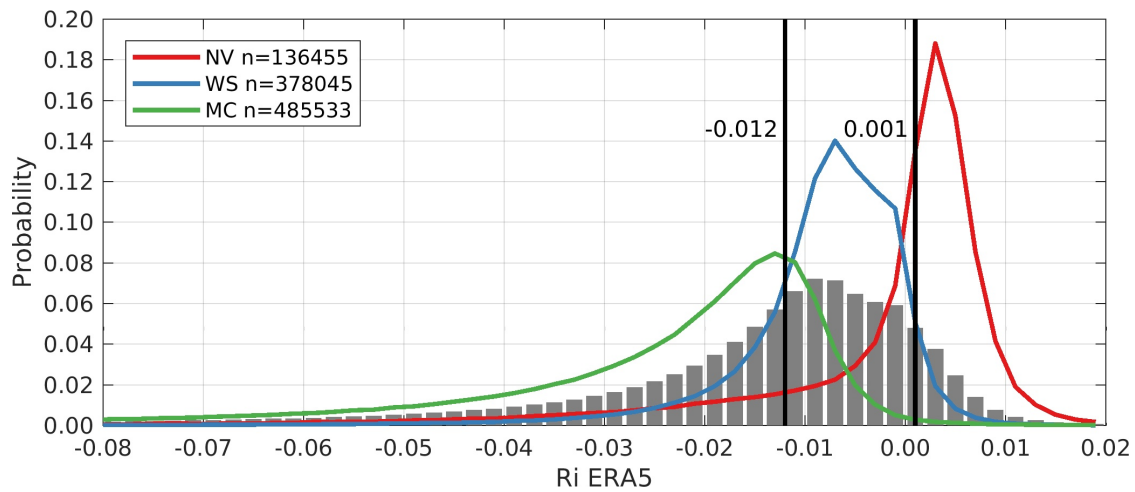
**Figure S2.** (a) PDFs of the MABL $Ri$ estimated from ERA5 for cells (unstable), streaks (near stable), and negligible atmospheric variability (stable) detection from SAR. The dashed lines represent the SAR sampling when using the FFT energy in the band of 0.8 to 4 km.



**Figure S3.** (a) PDFs of the MABL $Ri$ estimated from ERA5 for cells (unstable), streaks (near stable), and negligible atmospheric variability (stable) detection from SAR using a detection probability threshold of 50%.
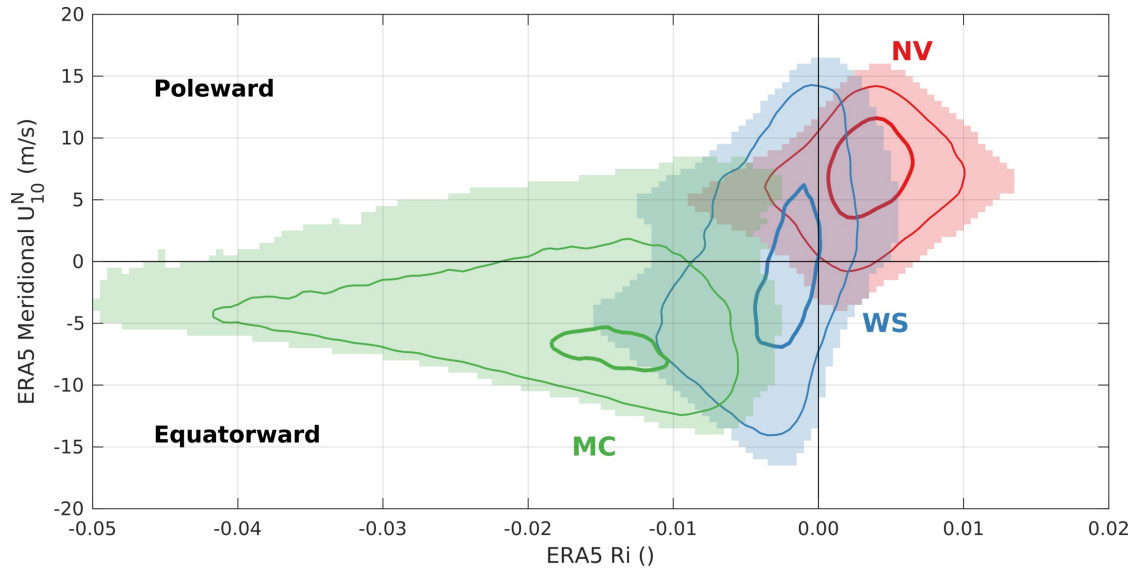
**Figure S4.** Occurrence of the $Ri$ versus meridional (N-S) wind speed ($U_{10}^N$) for the three SAR classes for latitudes greater than $25°N/S$. The green, blue, and red shading represents $10\%$ of the maximum bin within this $Ri$-$U_{10}^N$ space for MC, WS, and NV classes respectively. The thin and thick contours represent 25 and 75 percentiles respectively. The detection probability threshold is $50\%$ rather than $95\%$ as in the main text.
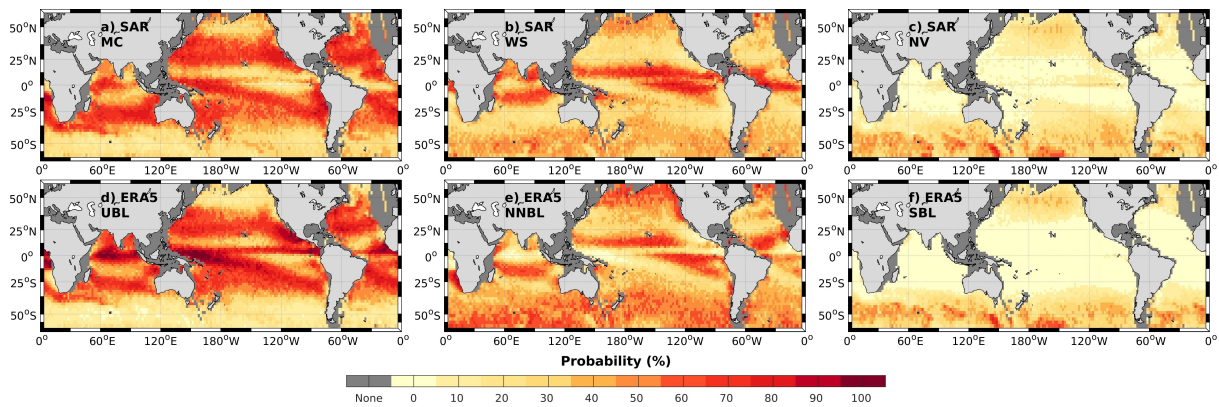
June 7, 2022, 5:18am

**Figure S5.** Relative occurrence rate between SAR-detected MC, WS, and NV events, top panels (a-c), using selected 2016-2019 S-1 data. Results are calculated for 2° bins. Panels d-f show the same events but mapped using ERA5 unstable, near-neutral and stable boundary layer stratification classes based on $Ri$ as defined in the main text. The detection probability threshold is 50% rather than 95% as in the main text.
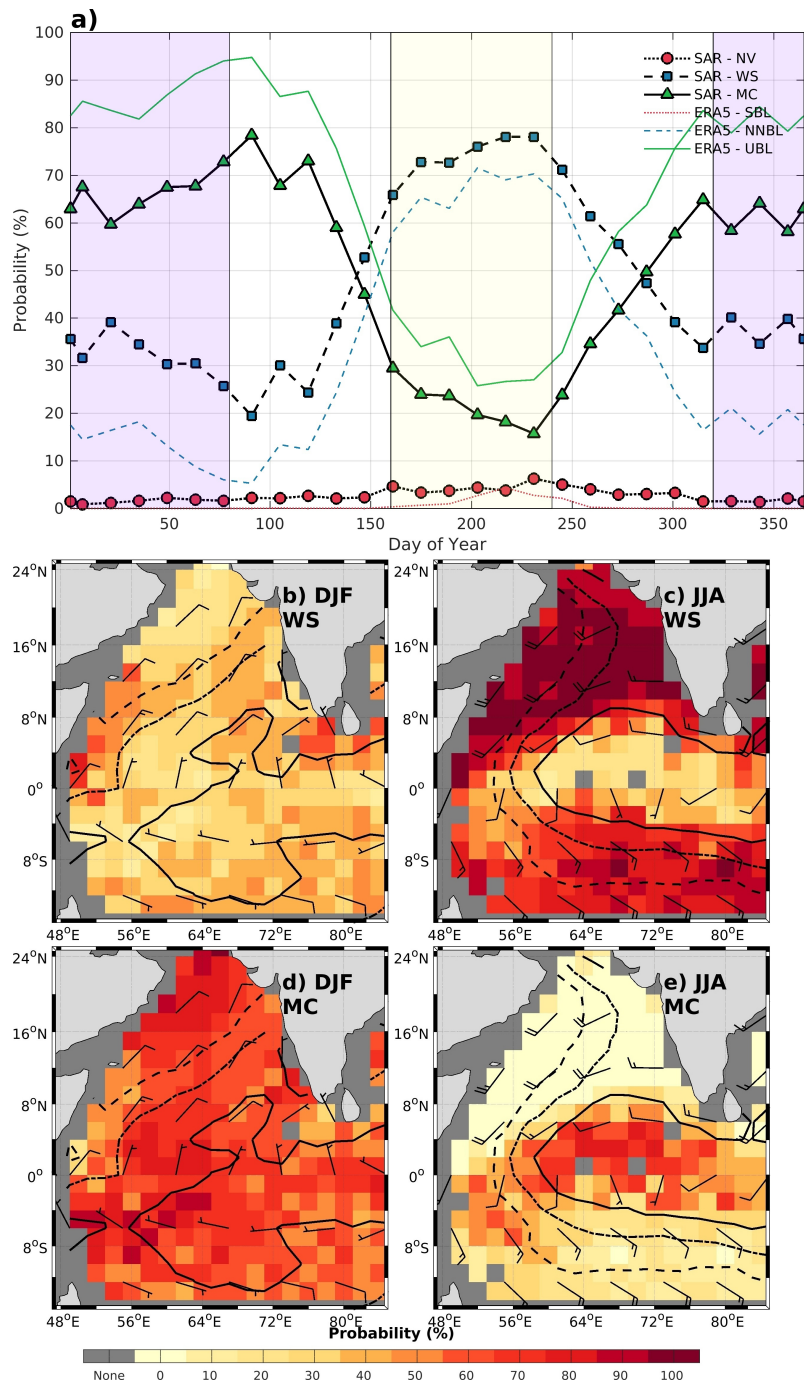
**Figure S6.** Relative occurrence rates between SAR-detected MC, WS, and NV images in the western Indian Ocean. Panel a) gives the biweekly regional averages. It also shows time series of averages among the three study BL stratification classes using ERA5 $Ri$ data. The maps in 2∘ bin-averaged seasonal WC and MC rates from the winter (Dec.- Feb., DJF) and summer (Jun.-Aug.), JJA) monsoon periods. The surface wind vectors are given as the barbs (direction from) where a full barb is 10 knots. The $SST_v$ 27, 28, and 29∘C contours are given as the solid, dash-dot, and dotted lines. These wind and $SST_v$ information are obtained by averaging ERA5 over our larger overall WV2 dataset and not the 27% of selected images to show the climatology. The detection probability threshold is 50% rather than 95% as in the main text.
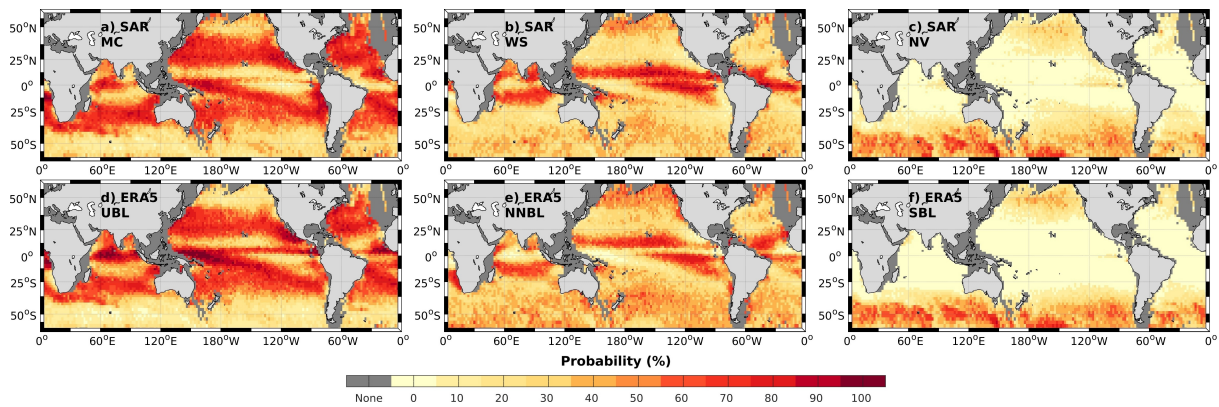
**Figure S7.**    Relative occurrence rate between SAR-detected MC, WS, and NV events, top panels (a-c), using selected 2016-2019 S-1 data. Results are calculated for 2° bins. Results are calculated for 2° bins. Panels d-f show the same for ERA5 unstable ($-0.012 < Ri$), near-neutral ($-0.012 < Ri < 0$) and stable boundary layer ($Ri > 0$) stratification classes.
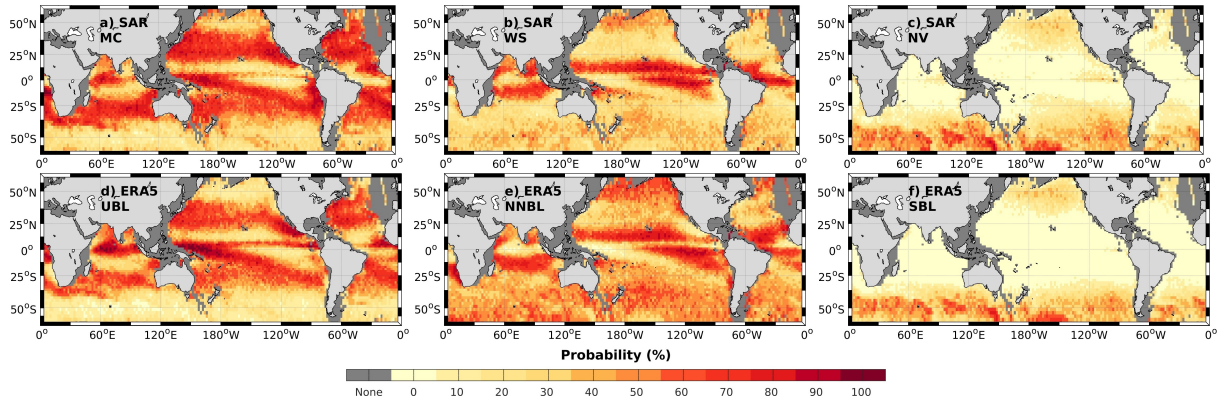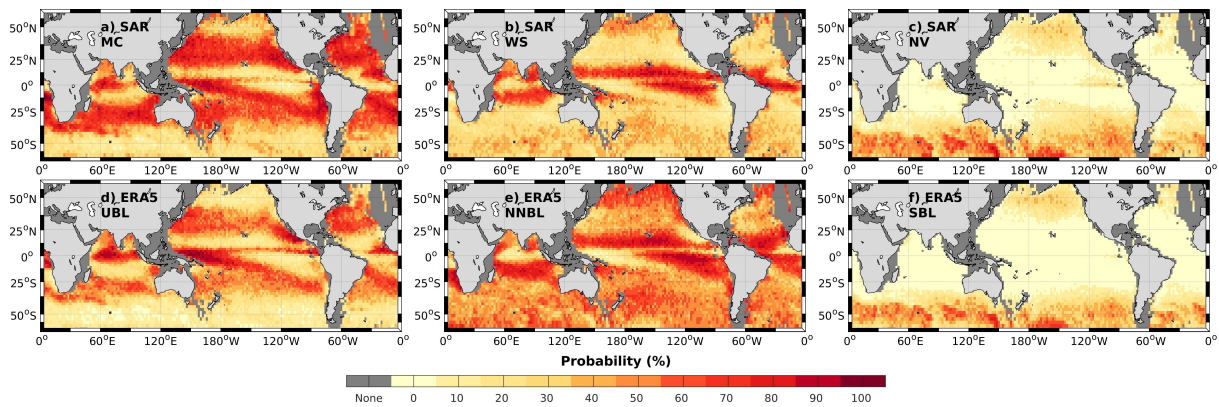
**Figure S8.** Relative occurrence rate between SAR-detected MC, WS, and NV events, top panels (a-c), using selected 2016-2019 S-1 data. Results are calculated for $2°$ bins. Results are calculated for $2°$ bins. Panels d-f show the same for ERA5 unstable $(-0.014 < Ri)$, near-neutral $(-0.014 < Ri < 0.01)$ and stable boundary layer $(Ri > 0.01)$ stratification classes.

**Figure S9.** Relative occurrence rate between SAR-detected MC, WS, and NV events, top panels (a-c), using selected 2016-2019 S-1 data. Results are calculated for 2° bins. Results are calculated for 2° bins. Panels d-f show the same for ERA5 unstable $(-0.016 < Ri)$, near-neutral $(-0.016 < Ri < 0.01)$ and stable boundary layer $(Ri > 0.01)$ stratification classes.
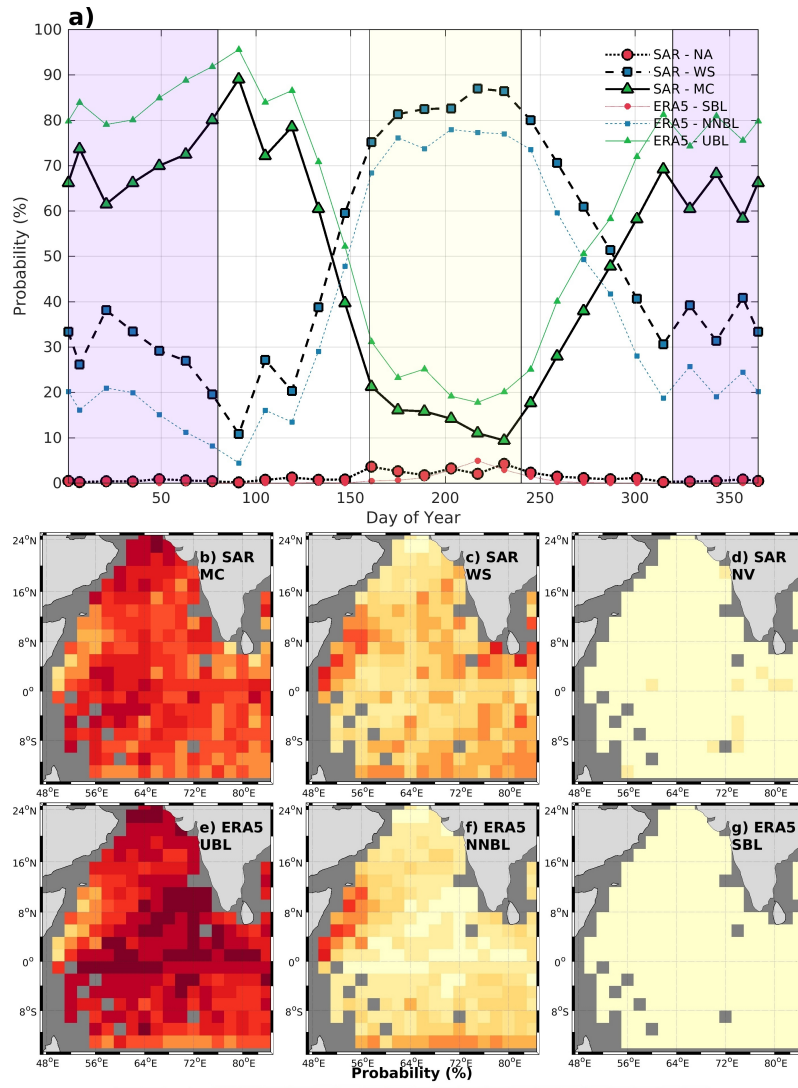
**Figure S10.** Relative occurrence rates between SAR-detected MC, WS, and NV images in the western Indian Ocean. Panel a) gives the biweekly regional averages. It also shows time series of averages among the three study BL stratification classes using ERA5 $Ri$ data. Relative occurrence rate between SAR-detected MC, WS, and NV events in panels (a-c), using selected 2016-2019 S-1 data. The maps in 2° bin-averaged seasonal WC and MC rates from the winter (Dec.-Feb., DJF) monsoon period. Panels d-f show the same events but mapped using ERA5 unstable, near-neutral and stable boundary layer stratification classes based on $Ri$ as defined in the main text.
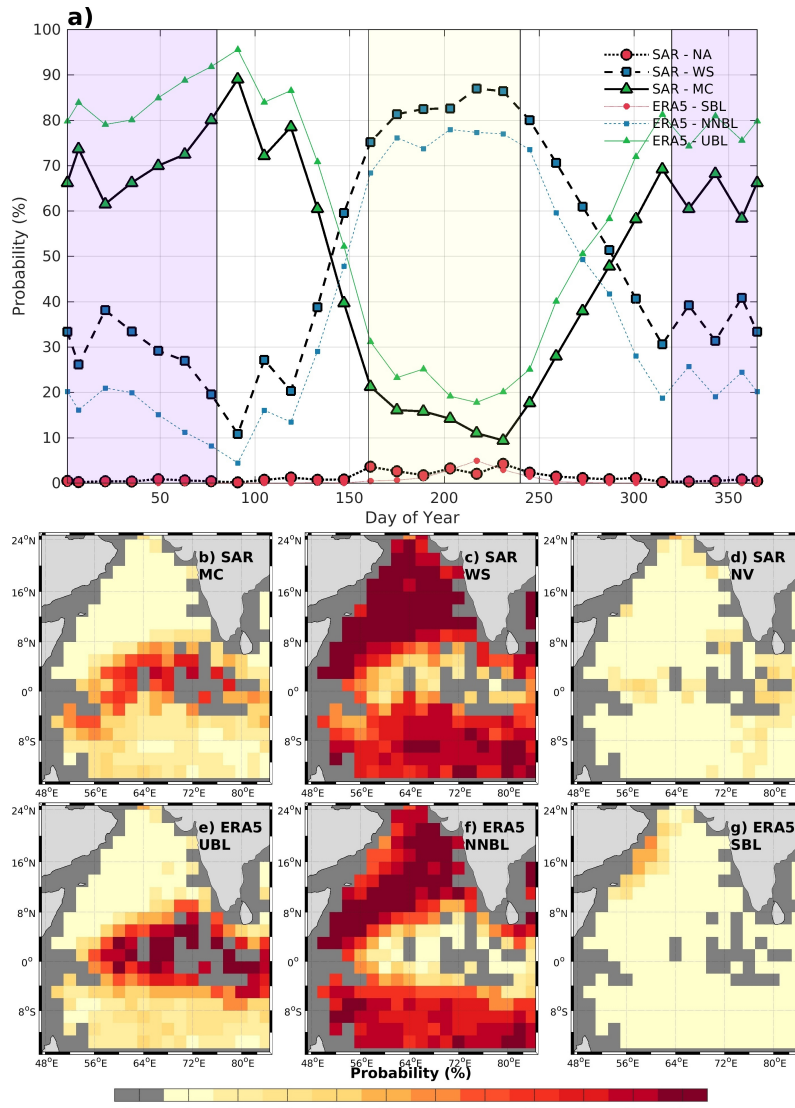
**Figure S11.** The same as Fig. SS10 except for the summer (Jun.-Aug., JJA) monsoon period.